Exogenous Fatty Acid Hydroperoxide Perception as Elicitor Is Related to Modulation of Plant Plasma Membrane Structure

Estelle Deboever[1], Géraldine van Aubel[2], Valeria Rondelli[3], Alexandros Koutsioumpas[4], Marion Mathelie-Guinlet[5], Yves Dufrêne[5], Marc Ongena[1], Laurence Lins[1], Pierre Van Cutsem[6], Marie-Laure Fauconnier[1], and Magali Deleu[1]

[1]University of Liege
[2]Fytofend S.A.
[3]Università degli Studi di Milano
[4]Heinz Maier-Leibnitz Zentrum
[5]Université catholique de Louvain
[6]Université de Namur Departement de Biologie

March 2, 2021

Abstract

Fatty acid hydroperoxides (HPOs) are amphiphilic molecules naturally produced by plants in stressed conditions and involved in plant immunity as signalling molecules. Although some studies report their potential use as exogenous biocontrol agents for plant protection, evaluation of their efficiency in planta is lacking and no information is available about their mechanism of action. In this work, the potential of two HPO forms, 13-HPOD and 13-HPOT, as plant defence elicitors and the underlying mechanism of action are investigated. Both HPOs trigger Arabidopsis innate immunity. They increase plant resistance to the pathogenic fungi Botrytis cinerea and activate early immunity-related defence responses, like ROS production. As our previous study has suggested that HPOs are able to interact with the plant plasma membrane (PPM) lipid fraction, we have further investigated the effects of HPOs on biomimetic PPM structure using complementary biophysics tools. Results show that HPO insertion into PPM impacts its global structure without solubilizing it. 13-HPOT, with an additional double bond compared to 13-HPOD, exerts a higher effect by fluidifying and reducing the thickness of the bilayer. Correlation between biological assays and biophysical analysis suggests that lipid amphiphilic elicitors that directly act on membrane lipids might trigger early plant defence events.

Exogenous Fatty Acid Hydroperoxide Perception as Elicitor Is Related to Modulation of Plant Plasma Membrane Structure

DEBOEVER Estelle [1,2,8], VAN AUBEL Géraldine[3],[8], RONDELLI Valeria[4], KOUTSIOUMPAS Alexandros[5], MATHELIE-GUINLET Marion [6], DUFRENE Yves F.[6], ONGENA Marc [7], LINS Laurence[1], VAN CUTSEM Pierre [3,8], FAUCONNIER Marie-Laure [2*] and DELEU Magali [1*]

[1]Laboratory of Molecular Biophysics at Interfaces, Gembloux Agro-Bio Tech, University of Liège, 2, Passage des Déportés, B-5030 Gembloux, Belgium

[2]Laboratory of Natural Molecules Chemistry, Gembloux Agro-Bio Tech, University of Liège, 2, Passage des Déportés, B-5030 Gembloux, Belgium

[3]Research Unit in Plant Cellular and Molecular Biology, University of Namur, Rue de Bruxelles, 61, B-5000 Namur, Belgium

[4] Department of Medical Biotechnologies and Translational Medicine, Università degli Studi di Milano, L.I.T.A., Via F.lli Cervi 93, 20090 Segrate, Italy

[5]Jülich Centre for Neutron Science (JCNS) at Heinz Maier-Leibnitz Zentrum (MLZ), Forschungszentrum Jülich GmbH, Lichtenbergstrasse 1, 85748 Garching, Germany

[6]Institute of Biomolecular Science and Technology (IBST), Croix du sud 4-5/L7.07.06, B-1348 Louvain-la-Neuve, Belgium

[7]Microbial Processes and Interactions (MiPI), Gembloux Agro-Bio Tech, Université de Liège, 2, Passage des Déportés, B-5030 Gembloux, Belgium

[8]FytoFend S.A., rue Georges Legrand, 6, B-5032 Isnes, Belgium

***** Correspondence:*magali.deleu@uliege.be*(M.D.) +*marie-laure.fauconnier@uliege.be*(M-L. F.)

Author email address: Deboever Estelle: *e.deboever@fytofend.com* ; Van Aubel Géraldine: *geraldine.vanaubel@unamur.be* ; Rondelli Valeria: *valeria.rondelli@unimi.it* ; Koutsioumpas Alexandros:*a.koutsioumpas@fz-juelich.de* ; Mathelie-Guinlet Marion:*marion.mathelie@uclouvain.be* ; Dufrêne Yves:*yves.dufrene@uclouvain.be* ; Ongena Marc:*marc.ongena@uliege.be* ; Lins Laurence: *l.lins@uliege.be* ; Van Cutsem Pierre: *pierre.vancutsem@unamur.be* ; Fauconnier Marie-Laure:*marie-laure.fauconnier@uliege.be*; Deleu Magali:*magali.deleu@uliege.be.*

Date of submission:

Number of Tables: 0 - Number of Figures: 5

Word count: 5329

Supplementary data: Figures: 2 - Tables: 2

Short Title : Plant hydroperoxide eliciting activity is linked to PPM modulation

Highlight : Modulation of the lipid dynamics of plant plasma membrane by exogenous fatty acid hydroperoxide oxylipins triggers early defence events like ROS production leading to plant resistance against pathogens

Abstract: Fatty acid hydroperoxides (HPOs) are amphiphilic molecules naturally produced by plants in stressed conditions and involved in plant immunity as signalling molecules. Although some studies report their potential use as exogenous biocontrol agents for plant protection, evaluation of their efficiency *in planta* is lacking and no information is available about their mechanism of action. In this work, the potential of two HPO forms, 13-HPOD and 13-HPOT, as plant defence elicitors and the underlying mechanism of action are investigated. Both HPOs trigger *Arabidopsis* innate immunity. They increase plant resistance to the pathogenic fungi *Botrytis cinerea* and activate early immunity-related defence responses, like ROS production. As our previous study has suggested that HPOs are able to interact with the plant plasma membrane (PPM) lipid fraction, we have further investigated the effects of HPOs on biomimetic PPM structure using complementary biophysics tools. Results show that HPO insertion into PPM impacts its global structure without solubilizing it. 13-HPOT, with an additional double bond compared to 13-HPOD, exerts a higher effect by fluidifying and reducing the thickness of the bilayer. Correlation between biological assays and biophysical analysis suggests that lipid amphiphilic elicitors that directly act on membrane lipids might trigger early plant defence events.

Keywords: Elicitor, Fatty Acid Hydroperoxide, Molecular Mechanism, Oxidative Burst, Oxylipin, Plant Defence, Plant Plasma Membrane.

Abbreviations : (13-HPOD) 13-hydroperoxy- 9,11-octadecadienoic acid; (13-HPOT) 13-hydroperoxy-9,11,15-octadecatrienoic acid; (AFM) atomic force microscopy; (CMC) critical micelle concentration; (COS) chitooligosaccharides, (d_{62}DPPC) 1,2-dipalmitoyl-d62-sn-glycero-3-phosphocholine; (DAMP)

damage-associated molecular pattern; (DMSO) dimethylsulfoxide; (Flg22) flagellin; (GIPC) glycosyl-inositol-phosphoryl-ceramide; (GluCer) glucosylceramide; (GP) generalized polarization; (HPO) fatty acid hydroperoxide; (ISR) induced systemic resistance; (LOX-1) Lipoxidase from Glycine max (soybean) type I-B; (MLV) multilamellar vesicles; (MS) Murashige and Skoog medium; (NR) neutron reflectometry; (OGA) oligogalacturonides; (PAMP) pathogen-associated molecular pattern; (PLPC) 1-palmitoyl-2-linoleoyl-sn-glycero-3-phosphocholine; (POX) peroxidase; (PPM) plant plasma membrane; (PRR) pattern recognition receptor; (RBOH) respiratory burst oxidase homolog; (RLU) relative light unit; (RT) room temperature; (SAR) systemic acquired resistance; (SLB) supported lipid bilayer; (SLD) scattering length density; (SUV) small unilamellar vesicle; (THSD) Tukey honest significant differences; (TRIS) tri(hydroxymethyl)aminomethane.

Introduction

Since several chemical pesticides have been shown to be detrimental on human health and ecosystems, considerable research has been done to find more environment-friendly plant protection solutions (Carvalho, 2017; Gay, 2012; Hernández et al., 2013; Wang et al., 2013). Elicitors, defined as molecules able to stimulate defence responses in a host plant, are one of the emerging alternatives (Henry et al., 2012; Paré et al., 2005; Thakur and Sohal, 2013). They can have a biological origin, be derived from plants (termed as Damage-Associated Molecular Patterns (DAMPs)) or microorganisms (referred as Microbe-Associated Molecular Patterns (MAMPs) or Pathogen-Associated Molecular Patterns (PAMPs)) (Malik et al., 2020; Yu et al., 2017) or even be chemically synthesized (Luzuriaga-Loaiza et al., 2018). They can be of different chemical natures like carbohydrate polymers, lipids, peptides and proteins (Boller and Felix, 2009; Jogaiah et al., 2019; Pršić and Ongena, 2020; Thakur and Sohal, 2013). Their perception by plant cells results in protection based on the activation of signalling cascades and defence mechanisms leading to the induction of plant immunity, like the systemic acquired resistance (SAR) and the induced systemic resistance (ISR) (Malik et al., 2020; Pršić and Ongena, 2020).

In addition to be a selective barrier between the cell and the extracellular medium, the plasma membrane is a sensor for modification of cellular environment and plays thus a key role in the recognition process of bioactive molecules. While many danger signals or invasion patterns are recognized by specific pattern recognition receptors within PPM (Pršić and Ongena, 2020; Schellenberger et al., 2019), some amphiphilic elicitors, like surfactin from *Bacillus* and rhamnolipids from *Pseudomonas* , have been strongly suggested to be perceived by the lipid fraction of PPM (Gerbeau-Pissot et al., 2014; Henry et al., 2011; Luzuriaga-Loaiza et al., 2018; Monnier et al., 2018). Recognition of elicitors by the plant cells first triggers early defence responses among which the release of reactive oxygen species (ROS) (superoxide anion ($O_2{}^{*-}$), hydrogen peroxide (H_2O_2) and hydroxyl radical ($^{*}OH$)), also known as the oxidative burst (Camejo et al., 2019; Mittler, 2017; Wang et al., 2019; Zaid and Wani, 2019).

HPOs are amphiphilic molecules naturally produced by plants in response to (a)biotic stresses by the oxidative catabolism of polyunsaturated fatty acids. They belong to the large family of plant oxylipins (Blee, 2002; Genva et al., 2019; Wasternack and Feussner, 2018). For years, HPOs, such as 9 or 13-hydroperoxy-9,11,15-octadecatrienoic acid (9 or 13-HPOT) and 9 or 13-hydroperoxy- 9,11-octadecadienoic acid (9 or 13-HPOD), have been extensively studied for their signalling properties (Deboever et al., 2020a). More recently, HPOs have emerged as a promising plant defence solution and their exogenous application to protect plants against phytopathogens has been considered (Deboever et al., 2020b; Graner et al., 2003; Prost et al., 2005). They display direct biocide activity against various plant bacteria and fungi (Prost et al., 2005). In our previous study (Deleu et al., 2019), we have also shown that HPOs are able to interact with PPM lipids and to perturb their lateral organization. We have hypothesized that by this interaction, HPOs could activate cellular signaling involved in plant defense mechanism.

In the present study, we first explored the potential of exogenously applied HPOs to protect *Arabidopsis thaliana* plants against*Botrytis cinerea* by a systemic signalling mechanism. Their eliciting activity was evaluated by measuring the ROS production by*Arabidopsis thaliana* cells in their presence. In a second part,

the molecular mechanism of HPO perception by the PPM was further investigated on plant biomimetic lipid systems by using a panel of complementary biophysical tools. More particularly, we analysed the effects of HPOs on the transversal organization and on the structure of the PPM bilayer.

Experimental procedures

Materials

As described in our previous works (Deboever et al., 2020b; Deleu et al., 2019; Fauconnier and Marlier, 1996), HPOs were enzymatically synthetized from the reaction of LOX-1 on linoleic (13-HPOD) or linolenic acid (13-HPOT). The purity (higher than 98%) was checked by high-performance liquid chromatography. For deuterated 13-HPOD, we used only deuterated reactants and solvents. Nuclear magnetic resonance and mass spectrometry were used for a full chemical characterization of the samples (data not shown).

1-palmitoyl-2-linoleoyl-sn-glycero-3-phosphocholine (PLPC), β-sitosterol, C16 glucosyl(ß) ceramide (d18:1/16:0) (GluCer), lipoxidase from Glycine max (soybean) type I-B (LOX-1), the linoleic and α-linolenic acids, 6-Dodecanoyl-N,N-dimethyl-2-naphthylamine (Laurdan), horseradish peroxidases, luminol were purchased from Sigma-Aldrich (Belgium). 1,2-dipalmitoyl-d62-sn-glycero-3-phosphocholine (d_{62}DPPC) was purchased from Avanti Polar Lipids (Italy). Deuterium oxide (D_2O) of 99.8% purity was purchased from ARMAR (Europa) GmbH. Chloroform and methanol were both purchased from Scharlau Lab Co. Dimethylsulfoxide (DMSO) and tri(hydroxymethyl)aminomethane (TRIS) were provided by Sigma Chemical. The ultrapure water was produced by Millipore systems available in our laboratory, the resistivity was 18.2 MΩ cm. The active substance COS-OGA was provided by FytoFend S.A. (Belgium) under the composition FytoSave® (12.5 g/L COS-OGA). *Botrytis cinerea* was grown on oat-based medium (25 g/L oat flour, 12 g/L agar) at room temperature.

Induction of ISR in *Arabidopsis thaliana*seedlings

The capacity of HPOs to trigger ISR was tested on *A. thaliana*infected by *B. cinerea* according to the procedure described in (Ongena et al., 2000). Seeds were sterilized with ethanol (70% v/v) and bleach (15% v/v) before multiple rinsing with sterile water, sowed in a square Petri Dish filled with agar medium (6-8 g/L) and transferred to a growth room at 22°C under a 16 h light/8 h dark photoperiod. After one week, seedlings were transferred to a sterile Araponics system filled with hydroponic solution (5 mL/10 L of Hydroponic Nutrient Solution 3-part Mix). After approximately 5 weeks in the growth room, the plants were transferred to 10 mL vials containing 10 mL hydroponic and kept in the dark wrapped in aluminium foil then transferred to adapt for one day before elicitation. The next day, half of the plants were treated in vials with 10 mL hydroponic solution supplemented with 20 mM HPOs in 1% DMSO. The other half (control) was treated with 10 mL hydroponic solution with 1% DMSO. After 24 h, four leaves of each plant were infected with *B. cinerea* . A 3-µL droplet containing 2 500 spores was deposited on the adaxial face of each leaf. Four days after inoculation, the disease was scored as the percentage of *B. cinerea* lesions having extended beyond the inoculum drop zone to produce spreading lesions (Ongena et al., 2007, 2000). Three independent experiments were carried out, with 8 plants per treatment.

Production of H_2O_2 by *Arabidopsis thaliana*

Photoautotrophic cell suspensions from *A. thaliana* strain Landsberg erecta ecotype were cultured on a rotary shaker at 100 rpm, in Murashige and Skoog (MS) medium (4.4 g/L) with 0.5 mg/L naphthalene acetic acid, 0.05 mg/L kinetin, pH 5.7 and maintained at 24°C with approximately 2% CO_2 under a 16 h/8 h light/dark photoperiod. H_2O_2 production was assessed using luminol-dependent chemiluminescence on seven-day-old cells directly after the addition of the elicitors in the growth medium, according to the method described by Baker and Mock (Baker and Mock, 2004). Luminescence (relative light units, (RLU)) was

measured every three min for 90 min. Eight technical replicates were carried out for each test compound and three independent measurements were performed. Results were expressed as means ± standard deviations of the area under the H_2O_2 production curves. ROS production values were analysed using Tukey Honest Significant Differences (THSD) test for multiple comparisons ($p< 0.1$).

Calcein leakage

PLPC/sito/GluCer (60:20:20) small unilamellar vesicles (SUVs) were prepared as described previously (Deboever et al., 2020b; Deleu et al., 2013, 2019). PLPC, sitosterol and GluCer in proportion 60:20:20 were dissolved in a chloroform/methanol mixture (2/1, v/v). The solvent was evaporated under a gentle stream of nitrogen to obtain a dried lipid film which was maintained under vacuum overnight. 10 mM calcein in 10 mM TRIS-HCl buffer pH 7.4 was added to hydrate the dried lipid film. The lipid dispersion was maintained at 37°C for at least 1 h and vortexed every 10 min. 5 cycles of freeze-thawing were applied to spontaneously form multilamellar vesicles. To obtain SUVs, this suspension was sonicated to clarity (5 cycles x 2 min) using a titanium probe with 400W amplitude keeping the suspension in an ice bath. Finally, generated titanium particles were removed from SUV solution by centrifuging during 10 min at 6200 rpm. The unencapsulated calcein was removed from the SUV dispersion by the Sephadex G65 mini-column separation technique (Fu and Singh, 1999). The actual phospholipid content of each preparation was determined by phosphorus assay (Bartlett, 1958) and the concentration of liposomes was adjusted for each type of experiment to 5 µM in 10 mM TRIS-HCl buffer at pH 7.4.

Fluorescence was measured as previously described in (Bartlett, 1958) with a Perkin Elmer (model LS50B) fluorescence spectrometer equipped with polarizers. Total amount of calcein release was determined by adding Triton-X100 (0.2%) to a liposome suspension that dissolved the lipid membrane without interfering with the fluorescence signals. The emission and excitation wavelengths were set at 517 nm and 467 nm, respectively. A fluorescence signal of 750 µL of SUV was first recorded as a baseline, followed by the addition of 13-HPOD/T (at t=30 sec) in 7 different concentrations while continuing the recording for 900 s. The amount of calcein released after time t was calculated according to (Shimanouchi et al., 2009):

$$\text{RF } (\%) = 100 \ \frac{(I_t - I_o)}{(I_{\max} - I_o)}$$

where RF is the fraction of calcein released, I_o, I_t and I_{max} are the fluorescence intensities measured at the beginning of the experiment, at time t and after the addition of 0.2% Triton X-100, respectively. All experiments were carried out at least three times, each time with freshly prepared SUVs.

Laurdan generalized polarization

For Laurdan generalized polarization experiments, multilamellar vesicles (MLVs) were prepared based on (Deboever et al., 2020b; Parasassi and Gratton, 1995). PLPC, sitosterol and GluCer in proportion 60:20:20 were dissolved in a chloroform/methanol mixture (2/1, v/v). HPOs were added to the lipid mixture to reach a lipid:HPO molar ratio of 5:1. The solvent was evaporated under a gentle stream of nitrogen to obtain a dried lipid film which was maintained under vacuum overnight. The resulting film was hydrated with 10 mM Tris-HCl buffer at pH 7.4 prepared from Milli-Q water and 1 µL of Laurdan solution prepared in DMSO was added to reach a final concentration of 5 nM. The lipid dispersion was maintained at a temperature well above the transition phase temperature of the lipid for at least 1 h and vortexed every 10 min.

Fluorescence of Laurdan in MLVs was monitored at various temperatures (between 20 and 50°C by steps of 5°C) with a Perkin Elmer LS50B fluorescence spectrometer. Samples were placed in 10 mm pathlength quartz cuvettes under continuous stirring and the cuvette holder was thermostated with a circulating bath. Samples were equilibrated at each temperature for 10-15 min prior to the measurements.

The excitation wavelength was set to 360 nm (slit = 2.5 nm), and at least 10 measurements of emission intensities at 440 nm and 490 nm were recorded and averaged for each sample and the blank (DMSO) at each temperature. An emission spectrum from 400 nm to 600 nm (slit = 4.5 nm) was also recorded for each sample-temperature combination. Generalized polarization (GP) of Laurdan was then calculated according to (Harris et al., 2002; Parasassi et al., 1992):

$$\mathrm{GP} = \frac{I_{440} - I_{490}}{I_{440} + I_{490}}$$

where I_{440} and I_{490} are the blank-subtracted emission intensities at 440 nm and 490 nm, respectively. All experiments were carried out at least three times, each time with freshly prepared MLVs.

Neutron reflectometry

Neutron reflectometry (NR) measurements were performed at the MARIA neutron reflectometer (Mattauch et al., 2018) operated by Jülich Centre for Neutron Science at Heinz Maier-Leibnitz Zentrum in Garching (Germany) while using custom temperature-regulated (through a connected Julabo F12-ED circulator) liquid cells (Koutsioubas, 2016). Two different wavelengths were used, 10 Å for the low-q region and 5 Å for the high-q region up to 0.25 $Å^{-1}$, with a 10% wavelength spread. Using a peristaltic pump combined with valves (flow rate ˜0.5 mL/min) solvent exchange was possible without moving the measuring cells from the instrument.

Specular NR measures the thickness and scattering length density (SLD) profile of layered structures along the surface normal (z). The SLD distribution along the normal, represented as $\varrho(z)$, is specific of the chemical composition of materials along the normal and depends on the coherent nuclear scattering lengths (b_i) of its constituent atoms and their number density along the normal (n_i (z)) so that $\varrho(z) = [?]_i b_i\ n_i\ (z)$. In reflectivity data measurements, the intensity of reflected neutrons is recorded relatively to the incident beam as a function of the momentum transfer vector ($q = 4\pi \sin\vartheta/\lambda$), where ϑ is the incidence angle and λ the wavelength of incident neutrons. The variation of reflectivity as a function of momentum transfer $R(q_z)$ is related to the square modulus of the one-dimensional Fourier transform of the SLD profile along the normal to the interface ($\varrho(q_z)$) through the relation:

$$R(q_z) \sim (16\pi / q_z)|\rho(q_z)|$$

Following the characterization by neutron reflectivity of silicon/solution interface, we deposited by vesicle fusion the membrane of interest (Koutsioubas et al., 2017). After its full characterization in 150 mM NaCl solutions in D_2O and H_2O, 2 µg of 13-HPOD/T (a concentration lower than their critical micelle concentration (CMC = 25.4 ± 1.9 µM and 24.0 ± 1.3 µM for 13-HPOT and 13-HPOD, respectively, according to (Deleu et al., 2019)), deuterated or not depending on the membrane studied, were injected in the measuring cell (6 mL total volume). Reflectivity was measured after letting the systems equilibrate for 1 h, again in the two contrasts condition with 10 mM Tris (pH 7.4).

To analyse the specular reflection data, the interface is modelled as a series of parallel layers where each layer is characterized by an average SLD and a thickness. Based on these parameters, a model reflectivity profile is calculated by means of the optical matrix method (Névot and Croce, 1980). The interfacial roughness between two consecutive layers is included in the model by the Abeles method, as described by Nevot and Croce (Névot and Croce, 1980).

Finally, the calculated model profile is compared to the measured profile and the quality of the fit is assessed by using the χ^2 in minimum-squares method. NR is a technique suited to collect structural information about the different layers of the studied membrane (Rondelli et al., 2019). Thus, the silicon support and the bulk water are seen as bulk infinite layer, the silicon oxide layer, the water layer between the silicon oxide and the

membrane and the diverse hydrophilic/hydrophobic layers of the lipid membranes are modelled as defined layers with a proper thickness, roughness with respect to the previous layer, compactness, composition and consequently contrast. Supported lipid bilayers (SLB) were formed using both the same lipid mixture as previously (PLPC/sito/GluCer in molar ratio 60/20/20) and d_{62}DPPC. Injections were done at 47°C and measurements at room temperature (RT). The reflectivity profile of the silicon support and of the samples has been measured in different contrasts (H_2O and D_2O) and data analysis was performed with the fit program MOTOFIT (Nelson, 2006). SLD used for the specific components are reported in Supplementary Data**Table S1** .

Atomic force microscopy

To probe the nanoscale effects of HPOs on lipid membranes, SLB (ternary mixture of PLPC/sito/GluCer (60/20/20)) were reconstructed on freshly cleaved mica substrates by allowing the fusion of a 2 mM lipid vesicles solution (V = 100 µL) at 55°C for 45 min. Samples were then left for thermalization at room temperature for 30 min without dewetting and immersed in 3 mL Tris buffer (pH 7.5).

To avoid damaging the samples, atomic force microscopy (AFM) images were obtained in the quantitative imaging (QI) mode of a JPK Nanowizard III setup, with a minimal applied force of 200 pN and a speed of 50 µm/s. Soft sharpened silicon nitride cantilevers (MSCT, Bruker) were used and calibrated before any experiment using the thermal noise method (k ˜ 0.02 N/m). HPOs, prepared in Tris buffer, were injected to reach a final concentration of 3 µM below their critical micellar concentration. AFM images were then recorded at different time points in different areas to follow the HPOs impact on the lipid bilayer.

Results

In planta protective effect of HPOs against phytopathogens

The capacity of HPOs to induce systemic resistance in *A. thaliana* against *B. cinerea* was tested under controlled conditions by treating plant roots with HPO solutions and inoculating plant leaves with the pathogen. The disease severity with HPO treatment was measured after 4 days and compared to controls (treatment with water containing 1% DMSO).

Treatment with both HPOs provided similar obvious disease reduction as shown by the decreased size of the lesions (**Figure 1**). About 40% of the plants had no symptoms. Given the experimental design (treatment and infection on two different plant organs), this cannot be a direct biocidal effect but rather a systemic signalling in the plant. One can therefore wonder about the signalling mechanism initiated by HPOs and more particularly their initial perception by the plant cells and the responses they induce.

Perception of HPOs and early defenses responses activation

Very often, ROS production is a biphasic process with a first transient phase within minutes after the infection and a second more intense and sustained phase that can last for many hours (Wang et al., 2019). This first wave, which is linked to the activation of early defence responses, has been investigated to determine whether the two HPOs are perceived by plants and can induce an immune response.

Cell suspensions cultures are a valuable model system for studying elicitor-induced defence reactions in plants and they easily allow studying early signalling events like oxidative bursts (Jogaiah et al., 2019; Khonon et al., 2011). Here, photoautotrophic *A. thaliana*cell suspensions were used to detect H_2O_2 production after treatment with HPOs. Extracellular ROS accumulation was detected using a luminol-based assay (Monnier et al., 2018; van Aubel et al., 2016). The elicitor FytoSave® was used as positive control as its active substance, COS-OGA made of pectin-derived oligogalacturonides (OGA) and chitooligosaccharides (COS), is known to induce a significant production of ROS at a concentration of 25 ppm (Ledoux et al., 2014; van

Aubel et al., 2018, 2016). A range of six different concentrations (0.5 µM to 100 µM) was tested and ROS production was monitored for 90 min.

The ROS production after 13-HPOD or 13-HPOT treatment was concentration-dependent (**Figure 2A).**It was higher than the controls, negative or positive, for concentrations 50 µM and 100µM. In those cases, the response to 13-HPOT treatment is higher than the 13-HPOD one. Also, the oxidative burst peak occurred quicker (30 min instead of 40 min) for 13-HPOT than for 13-HPOD (**Figure 2B).** Comparatively to COS-OGA, the kinetics of ROS production induced by HPOs in plant cells was slower (within 5 min only for COS-OGA *vs* 30-40 min for HPOs) but the oxidative burst lasted longer with a total duration of 60-70 min before returning to the basal level. Such long lasting response profile was also observed with synthetic rhamnolipid bolaforms, for which it was suggested that their perception occurred via the lipid fraction of the plasma membrane (Luzuriaga-Loaiza et al., 2018). On the contrary, the elicitor flagellin, known to be perceived by membrane pattern recognition receptors (Smith and Heese, 2014), induces a quicker oxidative burst initiated within 4-6 min with a peak at ˜10min (Yu et al., 2017), similarly to the OGA in the COS-OGA composition (Smith and Heese, 2014; van Aubel et al., 2013). The observation of different kinetic profiles for HPOs would suggest that a protein receptor is not directly involved in their recognition. Due to the ability of HPOs to interact with PPM lipids (Deleu et al., 2019), we hypothesized that the HPOs would rather be recognized via the lipid phase of the membrane.

Changes of PPM biophysical properties induced by HPOs

The interaction of HPOs with PPM characteristic lipids has already been found to modify the lateral organization of membrane bilayer in terms of lipid domain size and distribution (Deleu et al., 2019). It is also known that the plant sphingolipid GluCer is a privileged partner for the interaction and that 13-HPOT has a higher interaction affinity than 13-HPOD.

In the present study, further analysis of the effects of HPOs interaction with lipids on PPM structure was carried out. Simplified biomimetic models with two different lipid compositions were studied, the first mimicking the PPM, namely PLPC:sito:GluCer (60/20/20), and the second made of d_{62}DPPC, a classic deuterated model.

Effect of HPOs on membrane permeability

First, we have investigated the ability of HPOs to permeabilize model membranes by measuring the release of calcein. If the membrane is permeabilized by a bioactive molecule, the self-quenched calcein initially encapsulated within the LUV is released into the external medium and gives rise to an increase of fluorescence emission. Very little permeabilization effect was observed (values less than 10%) for both HPOs on the PLPC:sito:GluCer membrane model (**Figure S1**) suggesting that HPOs would not derive their mode of action from a mechanism of solubilization of the membrane or pore formation, but rather a more subtle modification of the membrane organization that could lead to the activation of a signalling cascade.

Change in bilayer fluidity induced by HPOs

The effect of HPOs on the bilayer fluidity was investigated by monitoring the lipid phase-dependent emission spectrum shift of Laurdan, a fluorescent probe that readily locates at the hydrophilic/hydrophobic interface of bilayers (Harris et al., 2002; Sanchez et al., 2007). Its fluorescence depends on the physical state of the environment. When present in a gel phase bilayer, its maximum fluorescence intensity is close to 440 nm emission wavelength. When the bilayer is in a fluid state, the Laurdan maximum fluorescence is observed at higher wavelengths (around 490 nm). This "red-shift" phenomenon is due to a higher quantity and mobility of the water molecules located around the probe. This is directly related to the lower order within the bilayer and is measured by the Generalized Polarization (GP): a decreasing GP value corresponds to a higher fluidity of the bilayer (Parasassi et al., 1991). This method has been previously applied for investigating the effect

of drugs, natural herbicides or other elicitors on lipid membrane organization (Deleu et al., 2013; Furlan et al., 2020; Lebecque et al., 2019; Sautrey et al., 2014).

The effect of HPOs on PLPC:sito:GluCer MLV membrane fluidity was investigated for a range of temperatures from 20°C to 50°C (**Figure 3**). In presence of 13-HPOT, the Laurdan GP values decreased significantly compared to those observed on pure MLVs with no significant effect of temperature. This indicates a fluidifying effect of 13-HPOT on the bilayer. On the contrary, 13-HPOD did not induce significant change in lipid order at any temperature as its curve almost superimposes to that of pure PLPC:sito:GluCer vesicles.

Effect of HPOs on the bilayer transversal structure

The effect of HPOs on the transversal structure of PPM was analysed by NR, a technique of choice to study the transverse structure of layered samples within a few Å resolution (Mattauch et al., 2018) and to evidence the structural effects of the interaction of incoming molecules on biological membranes (Rondelli et al., 2018, 2016). Neutrons interaction with matter depends on the isotopic species. Therefore, neutron-based experiments can profit by the use of deuterated molecules to enhance the visibility of molecules within a mixed complex system. As the lipids representative of the PPM are not commercially available in their deuterated form, d_{62}DPPC was used to form SLB and to highlight the presence and location of the H-bringing HPOs within the membrane.**Figure 4A-D** show the reflectivity curves together with their fittings in two contrasts and the corresponding fit parameters are summarized in **Figure 4E** . NR spectra were not drastically changed by the addition of HPOs. However, the spectra revealed that HPOs always insert into the outer membrane leaflet of the d_{62}DPPC SLB without flipping into the inner layer attached to the silicon block. A slight modification of the SLD profiles was observed while adding 13-HPOT but not with 13-HPOD. This gave rise to a small but significant decrease of the membrane thickness (approximately 2.5 Å) and roughness without modification of the solvent penetration, *i.e* ., no alteration of the bilayer. To confront these results, obtained on a d_{62}DPPC bilayer, to a more realistic PPM model, another experiment was performed with the deuterated version of 13-HPOD and the ternary mixture of non-deuterated lipids representative of PPM. It confirms that 13-HPOD interacts with PPM SLB and localizes on top of the outer leaflet without no major change of the membrane organization as observed from SLD profile and NR spectra (**Figure S2** and **Table S2**).

Lateral erosion of plant lipid bilayers by HPOs

To further analyse the effect of HPOs on the lipid bilayer organization, atomic force microscopy (AFM) was used to investigate their impact on the lateral nanoscale morphology of SLB. As shown in **Figure 5A** , the ternary mixture of plant lipids reconstituted in SLB did not reveal any phase separation within the thickness resolution limit of AFM (0.1 nm), rather homogeneous smooth patches (bright areas) distributed on the mica (dark areas). Though large patches were mainly found to cover the entire scanned area, defaults in the SLB were used as a "visualization control" to confirm the presence of the lipid bilayer. Its thickness of ˜4-5 nm, determined by measuring section profiles on the AFM height images, is in agreement with previous studies (**Figure 5B**) (Dufrêne and Lee, 2000; Mingeot-Leclercq et al., 2008). The presence of the lipid bilayer was further confirmed by recording AFM force curves on areas of high *vs* low heights. A typical breakthrough of the lipid bilayer in the bright areas was observed while no such force signature was found in dark areas without lipid bilayers and associated with mica (**Figure 5C**).

After confirming the presence of the SLB, the sample was incubated with either 13-HPOT or 13-HPOD and AFM images were recorded every 10-15 min on a defined area. Incubation 13-HPOT or 13-HPOD resulted in a time-dependent alteration of the lipid patches (**Figure 5D**). Results showed that very small SLB patches (green arrows) disappeared after the addition of 13-HPOT, but that it had not a drastic impact on the large ones. On the contrary, 13-HPOD completely removed part of a large angular domain after 75 min (see green arrows). Nonetheless, after 75 min treatment with 13-HPOT, most of the lipid domains were thinner by approximately 2 nm as compared to the initial ones, suggesting that 13-HPOT flattened lipids or part of the upper leaflet in a time- and zone-dependent way, which was not observed for 13-HPOD (**Figure 5E-F**).

In brief, AFM studies revealed three major effects of HPOs on plant mimetic lipid bilayers (i) "erosion" of angular protrusions of large lipid domains, (ii) total erosion of small domains, and (iii) reduction in the thickness of the bilayer between 0.5 and 2 nm. 13-HPOT has also a greater effect on membrane organization and bilayer thickness than 13-HPOD.

General discussion and conclusion

In the present study, we show for the first time the potential of the exogenous application of acyl-hydroperoxides 13-HPOD and 13-HPOT to protect plants against phytopathogens. Both forms of HPOs applied on *A. thaliana* roots strongly reduce the size of the lesions further to the inoculation of*B. cinerea* on leaves. The protection effect without direct contact with the phytopathogen suggests their capacity to stimulate the plant immune system. Other phyto-oxylipins, the jasmonic acid precursor 12-oxo-phytodienoic acid and an [?]-ketol of octadecadienoic acid were recently identified as mobile signals responsible of ISR, originated in the plant roots and travelling into the plant vasculature (Wang et al., 2020). Our results show that exogenous application of 13-HPOD and 13-HPOT on *A. thaliana* cell suspension induces an important*in vitro* oxidative burst, known as a hallmark of elicitor recognition by the plant cells (Yu et al., 2017). Beyond their role as signals, we thus clearly demonstrate that HPO are recognized by the plant cells triggering a signalling cascade leading to ISR and plant protection against pathogens.

The extracellular ROS production is initiated earlier and lasts longer that the one observed with well-known proteic elicitors like flagellin for which recognition phenomenon involves direct interaction with membrane proteic receptors (Gomez-Gomez and Boller, 2002). But the kinetic profile is similar to the one observed for other amphiphilic lipid elicitors like surfactin and rhamnolipids (Henry et al., 2011; Jourdan et al., 2009; Luzuriaga-Loaiza et al., 2018; Ma et al., 2017) for which a mechanism linked to the perception by the lipid of the plasma membrane was suggested.

From our previous work (Deleu et al., 2019), we know that HPOs can interact with the lipid fraction of PPM. In the present study, NR analyses show that both HPOs are more preferably inserted in the outer leaflet of the bilayer. This interaction modifies the global morphology of the bilayer as shown by AFM where bilayer erosion is observed for both HPOs. 13-HPOT has a higher impact on the PPM structure, but does not affect the integrity of the membrane according to the calcein release assays. Its insertion further reduces the thickness of the bilayer according to the NR and AFM data and fluidifies it more according to the Laurdan GP data than 13-HPOD. This difference between 13-HPOT and 13-HPOD could be explained by the presence of an additional double bond in 13-HPOT which gives it a greater structure rigidity. We postulate that this might force the lipids of the membrane outer leaflet to further reorganize compared to a more flexible molecule like 13-HPOD, and consequently could have a stronger impact on the dynamics of the membrane. The higher binding affinity of 13-HPOT compared to 13-HPOD for PPM bilayer (Deleu et al., 2019) could also enhance this reorganization effect.

The correlation between the higher ROS production and the higher impact on PPM lipid bilayer structure for 13-HPOT compared to 13-HPOD is in favour of our hypothesis that the PPM lipid fraction plays a key role in the recognition of HPOs giving rise to plant defence mechanisms. In the study of Sandor *et al.* (2016), it is demonstrated on *A. thaliana* and tobacco cells, that the induction of ROS by various elicitors including cryptogein, flagellin and an oligosaccharide, is concomitant to the increase in the relative proportion of membrane ordered domains (Sandor et al., 2016). According to them, the recognition of the elicitor at the plasma membrane level triggers the production of ROS which in turn reorganizes the membrane leading to an increase of ordered domains. But in the case of cryptogein, they have also suggested an inverse event sequence. Thanks to its capacity to interact with membrane sterols (Gerbeau-Pissot et al., 2014) and to mechanically trap them, cryptogein gives rise to a higher membrane fluidity which stimulates the ROS production. In agreement with this study, our results suggest that elicitors that directly act on membrane lipid dynamics and more particularly on the membrane fluidity are able to trigger early defence events like ROS production. But the complete molecular mechanistic view between the change of the membrane dynamics and the occurrence

of the oxidative burst is not yet identified. The formation of specific membrane lipid domains recruiting key signalling proteins (Gronnier et al., 2018) could be implicated. From our previous study (Deleu et al., 2019), we also know that plant membrane sphingolipids are privileged partners for HPO interaction. Therefore, the presence of glycosyl-inositol-phosphoryl-ceramides (GIPCs), the plant sphingolipids exclusively located in the outer leaflet of PPM and involved in the inter-leaflet coupling (Gronnier et al., 2016), could also play a role in the signal transduction.

In addition to their eliciting activity evidenced in the present study, HPOs also retain some antimicrobial activity against various phytopathogens (Deboever et al., 2020b). The dual effect of HPOs as well as the possibility to produce them at low cost (Fauconnier and Marlier, 1996) make them attractive compounds to be used as alternative to conventional pesticides for plant protection.

Author Contributions: Experiments design, E.D., M.D., V.R., A.K., M.M.M., M.O. and G.V.A..; experiments and data analysis, E.D., M.D., M.M.M., V.R. and G.V.A.; HPOs synthesis, and purification, E.D.; writing—original draft preparation, E.D.; writing—review and editing, all authors.

Data availability statement : The data supporting the findings of this study are available from the corresponding author, Magali Deleu, upon request.

Funding: E.D. is supported by a ¡¡ Fonds pour la formation a la Recherche dans l'Industrie et dans l'Agriculture ¿¿ (FRIA) grant (5100617F) from the FRS-FNRS (Fonds National de la Recherche Scientifique, Belgium). M.D., M. O. and L.L. thank the FRS-FNRS for their position as Senior Research Associates and for grant CDR (J.0014.08 and J.0086.18 projects). Work at the Universite Catholique de Louvain was supported by the National Fund for Scientific Research (FNRS) and the Research Department of the Communaute Francaise de Belgique (Concerted Research Action). Y.F.D. is a Research Director at the FNRS. This research was funded also by the 'Medical Biotechnologies and Translational Medicine Department' of the 'Universita degli Studi di Milano', grant number 'PSR2018' to V.R. This article was published with the support of the "Fondation Universitaire de Belgique".

Acknowledgments: The authors thank the financial support via the project from University of Liege (ARC-FIELD project 13/17-10). Authors also thank beamline MARIA Julich Centre for Neutron Science (JCNS) at Heinz Maier-Leibnitz Zentrum (MLZ, Garching, Germany) for allocation of beamtime. Acknowledgements are also due to FytoFend's research team for their logistic support in bioassays. Final thanks to Jelena Prisc for technical support and nice discussion on ISR and ROS experiment data measured *in planta* .

Conflicts of Interest: The authors declare no conflict of interest. The funders had no role in the design of the study; in the collection, analyses, or interpretation of data; in the writing of the manuscript, or in the decision to publish the results.

References

Baker, C.J., Mock, N.M., 2004. A method to detect oxidative stress by monitoring changes in the extracellular antioxidant capacity in plant suspension cells. Physiol. Mol. Plant Pathol. 64, 255–261.

Bartlett, G.R., 1958. Calorimetric Assay Phosphorylated for Free Glyceric Acids. J. Biol. Chem. 234, 469–471.

Blee, E., 2002. Impact of phyto-oxylipins in plant defense. Trends Plant Sci. 7, 315–321.

Boller, T., Felix, G., 2009. A Renaissance of Elicitors: Perception of Microbe-Associated Molecular Patterns and Danger Signals by Pattern-Recognition Receptors. Annu. Rev. Plant Biol. 60, 379–406.

Camejo, D., Guzman-cedeno, A., Vera-macias, L., Jimenez, A., 2019. Oxidative post-translational modi fi cations controlling plant-pathogen interaction. Plant Physiol. Biochem. 144, 110–117.

Carvalho, F.P., 2017. Pesticides, environment, and food safety. Food Energy Secur. 6, 48–60.

Deboever, E., Deleu, M., Mongrand, S., Lins, L., Fauconnier, M.-L., 2020a. Plant–Pathogen Interactions: Underestimated Roles of Phyto-oxylipins. Trends Plant Sci. 25, 22–34.

Deboever, E., Lins, L., Ongena, M., De Clerck, C., Deleu, M., Fauconnier, M.-L., 2020b. Linolenic fatty acid hydroperoxide acts as biocide on plant pathogenic bacteria : biophysical investigation of the mode of action. Bioorg. Chem. 100, 1–25.

Deleu, M., Deboever, E., Nasir, M.N., Crowet, J.-M., Dauchez, M., Ongena, M., Jijakli, H., Fauconnier, M.-L., Lins, L., 2019. Linoleic and linolenic acid hydroperoxides interact differentially with biomimetic plant membranes in a lipid specific manner. Colloids Surfaces B Biointerfaces 175, 384–391.

Deleu, M., Lorent, J., Lins, L., Brasseur, R., Braun, N., El Kirat, K., Nylander, T., Dufrene, Y.F., Mingeot-Leclercq, M.P., 2013. Effects of surfactin on membrane models displaying lipid phase separation. Biochim. Biophys. Acta - Biomembr. 1828, 801–815.

Dufrene, Y.F., Lee, G.U., 2000. Advances in the characterization of supported lipid films with the atomic force microscope. Biochim. Biophys. Acta - Biomembr. 1509, 14–41.

Fauconnier, M.L., Marlier, M., 1996. An efficient procedure for the production of fatty acid hydroperoxides from hydrolyzed flax seed oil and soybean lipoxygenase. Biotechnol. Tech. 10, 839–844.

Fu, F.N., Singh, B.R., 1999. Calcein permeability of liposomes mediated by type a botulinum neurotoxin and its light and heavy chains. J. Protein Chem. 18, 701–707.

Furlan, L., Laurin, Y., Botcazon, C., Rodr, N., Buchoux, S., 2020. Contributions and Limitations of Biophysical Approaches to Study of the Interactions between Amphiphilic Molecules and the Plant. Plants 9, 1–24.

Gay, H., 2012. Before and after silent spring: From chemical pesticides to biological control and integrated pest management-Britain, 1945-1980. Ambix 59, 88–108.

Genva, M., Obounou Akong, F., Andersson, M.X., Deleu, M., Lins, L., Fauconnier, M.L., 2019. New insights into the biosynthesis of esterified oxylipins and their involvement in plant defense and developmental mechanisms. Phytochem. Rev. 8, 343–359.

Gerbeau-Pissot, P., Der, C., Thomas, D., Anca, I.A., Grosjean, K., Roche, Y., Perrier-Cornet, J.M., Mongrand, S., Simon-Plas, F., 2014. Modification of plasma membrane organization in tobacco cells elicited by cryptogein. Plant Physiol. 164, 273–286.

Gomez-Gomez, L., Boller, T., 2002. Flagellin perception: A paradigm for innate immunity. Trends Plant Sci. 7, 251–256.

Graner, G., Hamberg, M., Meijer, J., 2003. Screening of oxylipins for control of oilseed rape (Brassica napus) fungal pathogens. Phytochemistry 63, 89–95.

Gronnier, J., Gerbeau-Pissot, P., Germain, V., Mongrand, S., Simon-Plas, F., 2018. Divide and Rule: Plant Plasma Membrane Organization. Trends Plant Sci. 23, 899–917.

Gronnier, J., Germain, V., Gouguet, P., Cacas, J.L., Mongrand, S., 2016. GIPC: Glycosyl inositol phospho ceramides, the major sphingolipids on earth. Plant Signal. Behav. 11, 1–7.

Harris, F.M., Best, K.B., Bell, J.D., 2002. Use of laurdan fluorescence intensity and polarization to distinguish between changes in membrane fluidity and phospholipid order. Biochim. Biophys. Acta - Biomembr. 1565, 123–128.

Henry, G., Deleu, M., Jourdan, E., Thonart, P., Ongena, M., 2011. The bacterial lipopeptide surfactin targets the lipid fraction of the plant plasma membrane to trigger immune-related defence responses. Cell. Microbiol. 13, 1824–1837.

Henry, G., Thonart, P., Ongena, M., 2012. PAMPs, MAMPs, DAMPs and others: an update on the diversity of plant immunity elicitors. Biotechnol. Agron. Societe ... 16, 12.

Hernandez, A.F., Parron, T., Tsatsakis, A.M., Requena, M., Alarcon, R., Lopez-Guarnido, O., 2013. Toxic effects of pesticide mixtures at a molecular level: Their relevance to human health. Toxicology 307, 136–145.

Jogaiah, S., Govind, S.R., Shetty, H.S., 2019. Role of Oomycete Elicitors in Plant Defense Signaling. In: Bioactive Molecules in Plant Defense. Springer International Publishing, pp. 59–74.

Jourdan, E., Henry, G., Duby, F., Dommes, J., Barthelemy, J.P., Thonart, P., Ongena, M., 2009. Insights into the defense-related events occurring in plant cells following perception of surfactin-type lipopeptide from Bacillus subtilis. Mol. Plant-Microbe Interact. 22, 456–468.

Khonon, M.A.R., Okuma, E., Hossain, M.O., Munemasa, S., Uraji, M., Nakamura, Y., Mori, I.C., Murata, Y., 2011. Involvement of extracellular oxidative burst in salicylic acid-induced stomatal closure in Arabidopsis. Plant Cell Environ. 34, 434–443.

Koutsioubas, A., 2016. Combined Coarse-Grained Molecular Dynamics and Neutron Ref ectivity Characterization of Supported Lipid Membranes. J. Phys. Chem. 120, 11474–11483.

Koutsioubas, A., Appavou, M.S., Lairez, D., 2017. Time-Resolved Neutron Reflectivity during Supported Membrane Formation by Vesicle Fusion. Langmuir 33, 10598–10605.

Lebecque, S., Lins, L., Dayan, F.E., Fauconnier, M., 2019. Interactions Between Natural Herbicides and Lipid Bilayers Mimicking the Plant Plasma Membrane. Front. Pharmacol. 10, 1–11.

Ledoux, Q., Van Cutsem, P., Markó, I.E., Veys, P., 2014. Specific localization and measurement of hydrogen peroxide in Arabidopsis thaliana cell suspensions and protoplasts elicited by COS-OGA. Plant Signal. Behav. 9, 1–6.

Luzuriaga-Loaiza, W.P., Schellenberger, R., De Gaetano, Y., Obounou Akong, F., Villaume, S., Crouzet, J., Haudrechy, A., Baillieul, F., Clément, C., Lins, L., Allais, F., Ongena, M., Bouquillon, S., Deleu, M., Dorey, S., 2018. Synthetic Rhamnolipid Bolaforms trigger an innate immune response in Arabidopsis thaliana. Sci. Rep. 8, 1–13.

Ma, Z., Ongena, M., Höfte, M., 2017. The cyclic lipopeptide orfamide induces systemic resistance in rice to Cochliobolus miyabeanus but not to Magnaporthe oryzae. Plant Cell Rep. 36, 1731–1746.

Malik, A.N.A., Kumar, I.S., Nadarajah, K., 2020. Elicitor and Receptor Molecules : Orchestrators of Plant Defense and Immunity. Int. J. Mol. Sci. 21, 963–997.

Mattauch, S., Koutsioubas, A., Ru, U., Korolkov, D., Fracassi, V., Daemen, J., Schmitz, R., Bussmann, K., Suxdorf, F., Wagener, M., Ka, P., Kleines, H., Fleischhauer-fuss, L., 2018. The high-intensity reflectometer of the Julich Centre for Neutron Science : MARIA research papers. J. Appl. Cristallogr. 51, 1–9.

Mingeot-Leclercq, M.P., Deleu, M., Brasseur, R., Dufrene, Y.F., 2008. Atomic force microscopy of supported lipid bilayers. Nat. Protoc. 3, 1654–1659.

Mittler, R., 2017. ROS Are Good. Trends Plant Sci. 22, 11–19.

Monnier, N., Furlan, A., Botcazon, C., Dahi, A., Mongelard, G., Cordelier, S., Clement, C., Dorey, S., Sarazin, C., Rippa, S., 2018. Rhamnolipids From Pseudomonas aeruginosa Are Elicitors Triggering Brassica napus Protection Against Botrytis cinerea Without Physiological Disorders. Front. Plant Sci. 9, 1–14.

Nelson, A., 2006. Co-refinement of multiple-contrast neutron / X-ray reflectivity data using MOTOFIT. J. Appl. Cristallogr. 39, 273–276.

Nevot, L., Croce, P., 1980. Caracterisation des surfaces par reflexion rasante de rayons X. Application a l'etude du polissage de quelques verres silicates. Rev. Phys. Appliquee 15, 761–779.

Ongena, M., Daayf, F., Jacques, P., Thonart, P., Benhamou, N., Paulitz, T.C., Belanger, R.R., 2000. Systemic induction of phytoalexins in cucumber in response to treatments with fluorescent pseudomonads. Plant Pathol. 49, 523–530.

Ongena, M., Jourdan, E., Adam, A., Paquot, M., Brans, A., Joris, B., Arpigny, J.L., Thonart, P., 2007. Surfactin and fengycin lipopeptides of Bacillus subtilis as elicitors of induced systemic resistance in plants. Environ. Microbiol. 9, 1084–1090.

Parasassi, T., De Stasio, G., Ravagnan, G., Rusch, R.M., Gratton, E., 1991. Quantitation of lipid phases in phospholipid vesicles by the generalized polarization of Laurdan fluorescence. Biophys. J. 60, 179–189.

Parasassi, T., Di Stefano, M., Ravagnan, G., Sapora, O., Gratton, E., 1992. Membrane aging during cell growth ascertained by laurdan generalized polarization. Exp. Cell Res. 202, 432–439.

Parasassi, T., Gratton, E., 1995. Membrane lipid domains and dynamics as detected by Laurdan fluorescence. J. Fluoresc. 5, 59–69.

Pare, P.W., Farag, M.A., Krishnamachari, V., Zhang, H., Ryu, C.M., Kloepper, J.W., 2005. Elicitors and priming agents initiate plant defense responses. Photosynth. Res. 85, 149–159.

Prost, I., Dhondt, S., Rothe, G., Vicente, J., Rodrigez, M.J., Kift, N., Carbonne, F., Griffiths, G., Esquerre-Tugaye, M.-T., Rosahl, S., Castresana, C., Hamberg, M., Fournier, J., 2005. Evaluation of the Antimicrobial Activities of Plant Oxylipins Supports Their Involvement in Defense against Pathogens. Plant Physiol. 139, 1902–1913.

Pršić, J., Ongena, M., 2020. Elicitors of Plant Immunity Triggered by Beneficial Bacteria. Front. Plant Sci. 11, 1–12.

Rondelli, V., Brocca, P., Motta, S., Messa, M., Colombo, L., Salmona, M., Fragneto, G., Cantu, L., Del Favero, E., 2016. Amyloidβ Peptides in interaction with raft-mime model membranes: A neutron reflectivity insight. Sci. Rep. 6, 1–11.

Rondelli, V., Cola, E. Di, Koutsioubas, A., Alongi, J., Ferruti, P., Ranucci, E., Brocca, P., 2019. Mucin Thin Layers : A Model for Mucus-Covered Tissues. Int. J. Mol. Sci. 20, 1–15.

Rondelli, V., Del Favero, E., Brocca, P., Fragneto, G., Trapp, M., Mauri, L., Ciampa, M.G., Romani, G., Braun, C.J., Winterstein, L., Schroeder, I., Thiel, G., Moroni, A., Cantu, L., 2018. Directional K + channel insertion in a single phospholipid bilayer: Neutron reflectometry and electrophysiology in the joint exploration of a model membrane functional platform. Biochim. Biophys. Acta - Gen. Subj. 1862, 1742–1750.

Sanchez, S.A., Tricerri, M.A., Gunther, G., Gratton, E., 2007. Laurdan Generalized Polarization : from cuvette to microscope. Mod. Res. Educ. Top. Microsc. 1007–1014.

Sandor, R., Der, C., Grosjean, K., Anca, I., Noirot, E., Leborgne-Castel, N., Lochman, J., Simon-Plas, F., Gerbeau-Pissot, P., 2016. Plasma membrane order and fluidity are diversely triggered by elicitors of plant defence. J. Exp. Bot. 67, 5173–5185.

Sautrey, G., Zimmermann, L., Deleu, M., Delbar, A., Machado, L.S., Jeannot, K., Van Bambeke, F., Buyck, J.M., Decout, J.L., Mingeot-Leclercq, M.P., 2014. New amphiphilic neamine derivatives active against resistant Pseudomonas aeruginosa and their interactions with lipopolysaccharides. Antimicrob. Agents Chemother. 58, 4420–4430.

Schellenberger, R., Touchard, M., Clément, C., Baillieul, F., Cordelier, S., Crouzet, J., Dorey, S., 2019. Apoplastic invasion patterns triggering plant immunity: plasma membrane sensing at the frontline. Mol. Plant Pathol. 20, 1602–1616.

Shimanouchi, T., Ishii, H., Yoshimoto, N., Umakoshi, H., Kuboi, R., 2009. Calcein permeation across phosphatidylcholine bilayer membrane: Effects of membrane fluidity, liposome size, and immobilization. Colloids

Surfaces B Biointerfaces 73, 156–160.

Smith, J.M., Heese, A., 2014. Rapid bioassay to measure early reactive oxygen species production in Arabidopsis leave tissue in response to living Pseudomonas syringae. Plant Methods 10, 1–9.

Thakur, M., Sohal, B.S., 2013. Role of Elicitors in Inducing Resistance in Plants against Pathogen Infection: A Review. ISRN Biochem. 2013, 1–10.

van Aubel, G., Buonatesta, R., Van Cutsem, P., 2013. COS-OGA, a new oligosaccharidic elicitor that induces protection against a wide range of plant pathogens. IOBC-WPRS Bull. 89, 403–407.

van Aubel, G., Cambier, P., Dieu, M., Van Cutsem, P., 2016. Plant immunity induced by COS-OGA elicitor is a cumulative process that involves salicylic acid. Plant Sci. 247, 60–70.

van Aubel, G., Serderidis, S., Ivens, J., Clinckemaillie, A., Legrève, A., Hause, B., Van Cutsem, P., 2018. Oligosaccharides successfully thwart hijacking of the salicylic acid pathway by Phytophthora infestans in potato leaves. Plant Pathol. 67, 1901–1911.

Wang, K. Der, Borrego, E.J., Kenerley, C.M., Kolomiets, M. V., 2020. Oxylipins Other Than Jasmonic Acid Are Xylem-Resident Signals Regulating Systemic Resistance Induced by Trichoderma virens in Maize. Plant Cell 32, 166–185.

Wang, S., Wang, Z., Zhang, Y., Wang, J., Guo, R., 2013. Pesticide residues in market foods in Shaanxi Province of China in 2010. Food Chem. 138, 2016–2025.

Wang, Y., Ji, D., Chen, T., Li, B., Zhang, Z., Qin, G., Tian, S., 2019. Production , Signaling , and Scavenging Mechanisms of Reactive Oxygen Species in Fruit – Pathogen Interactions. Int. J. Mol. Sci. 20, 1–12.

Wasternack, C., Feussner, I., 2018. The Oxylipin Pathways: Biochemistry and Function. Annu. Rev. Plant Biol. 69, 363–386.

Yu, X., Feng, B., He, P., Shan, L., 2017. From Chaos to Harmony: Responses and Signaling upon Microbial Pattern Recognition. Annu. Rev. Phytopathol. 55, 109–137.

Zaid, A., Wani, S.H., 2019. Reactive Oxygen Species Generation, Scavenging and Signaling in Plant Defense Responses. In: Bioactive Molecules in Plant Defense. Springer International Publishing, pp. 111–132.

6 *Figure legend*

Figure 1 - Disease severity distribution of B. cinerea on leaves from root-treated A. thaliana plants grown hydroponically. Treatments included control and two oxylipins: 13-HPOD and 13-HPOT. Scoring: 1, no symptoms; scoring 2, lesions smaller than 0.5 cm; scoring 3, lesions larger than 0.5 cm; scoring 4, beginning of sporulation on lesions. Results are based on three independent experiments. Standard deviation between the experiments is less than 7%.

Figure 2 - Early defense responses detection induced by HPOs in*A. thaliana* cells suspensions. **(A, B)** Production of ROS by controls and HPOs treated cells. **(A)** Mean area under H_2O_2 production curves for 90 min measurements. Data are based on three independent repetitions and error bars are the standard deviations of means. **(B)** One example of kinetics of ROS production for 13-HPOT, 13-HPOD, MS negative control and COS-OGA positive control.

Figure 3 - Evolution of Laurdan generalized polarization as a function of temperature for PLPC:sito:GluCer MLVs (50 µM) in the absence or presence of HPOs (lipid:HPO molar ratio 5:1).

Figure 4 - **(A,B)** Reflectivity curves (symbols), relatives fits (lines) and **(C,D)** obtained SLD profiles of the d_{62}DPPC membrane investigated in two contrasts before (green and orange) and after (bleu and red) the addition of 13-HPOT (left) and 13-HPOD (right) (lipid:HPO molar ratio 5:1). **(E)** Fit parameters of the d_{62}DPPC SLB alone and after the interaction with 13-HPOD/T. Parameters (Thickness, scattering length density (SLD), solvent penetration (Solv p) and roughness) correspond to a contemporary fit performed

on H_2O and D_2O solutions with 10mM Tris buffer (pH 7.4). Errors have been estimated by changing the parameters up to a variation of two in the χ^2. For each parameter, the maximum error found was kept. Measurements were carried out at room temperature.

Figure 5 - HPOs lead to lipids erosion. **A)** AFM topographic image of a PLPC:sito:GluCer (60:20:20) supported lipid bilayer (SLB), deposited on mica, and recorded in 10 mM Tris buffer at pH 7.5. **B)** Height profile of the SLB along the dashed line in (A) allowing the measurement of the sample thickness e. **C)**Force curves recorded on a bright area in (A) confirming the presence of the SLB, with a thickness e. **D)** AFM topographic images before (t_0) and after injection of 13-HPOT or 13-HPOD, at increasing incubation times. Scale bar 1 µm, same colour scale than in (A). **E-F)** Height density profiles recorded on small areas, defined as dashed squares in (D), of the PLPC:sito:GluCer bilayer before and after 75 min - incubation with 13-HPOT and 13-HPOD respectively.

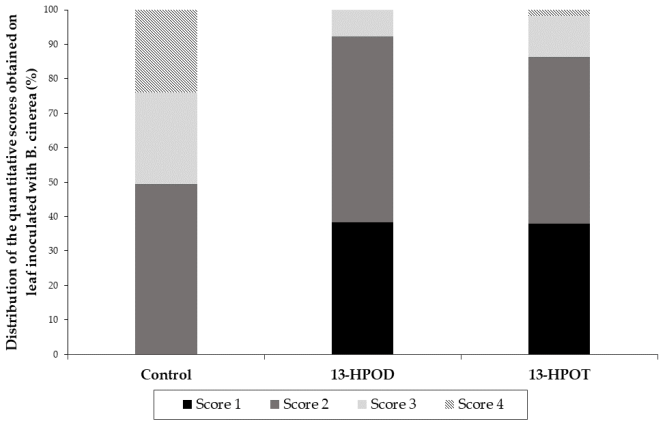

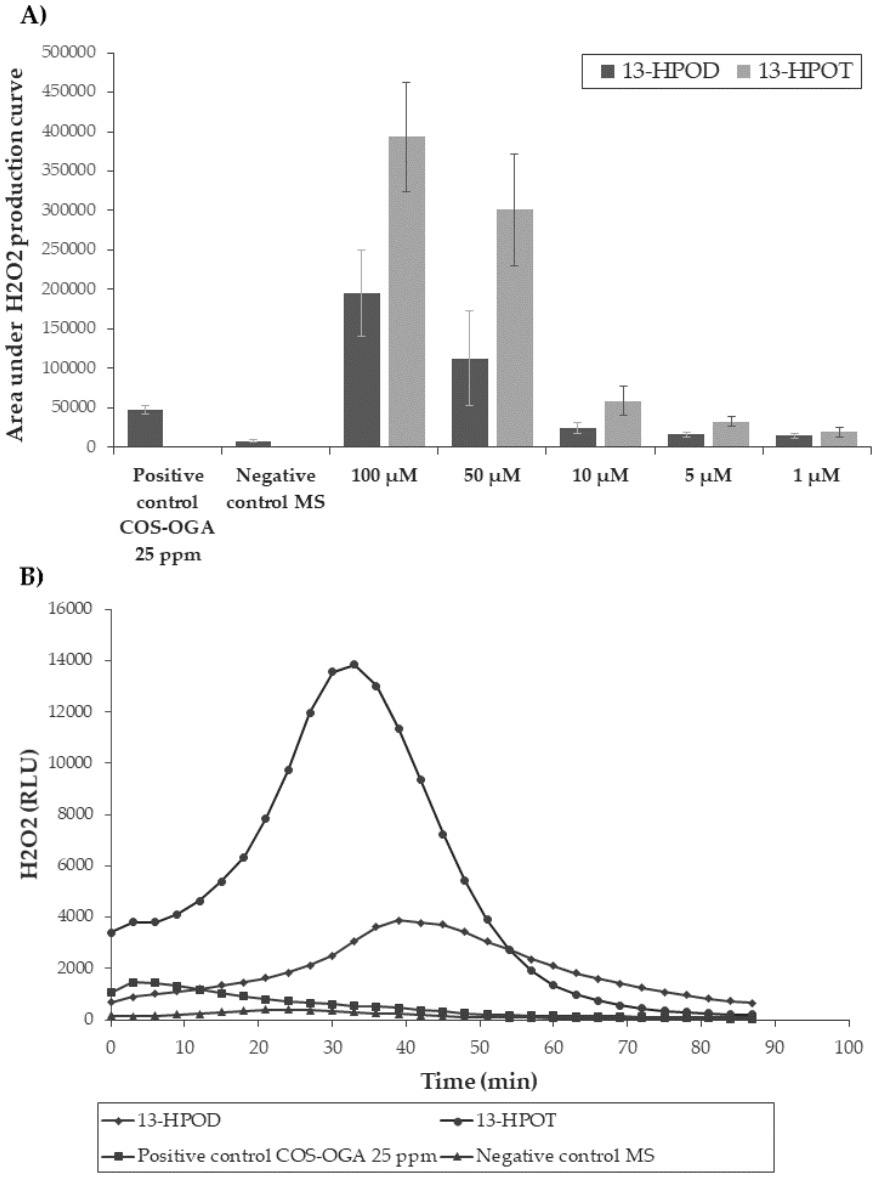

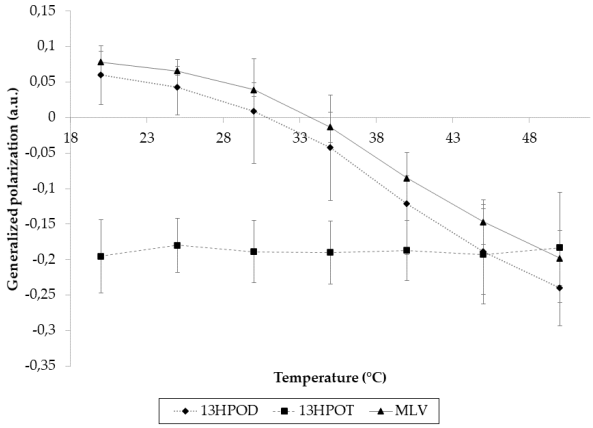

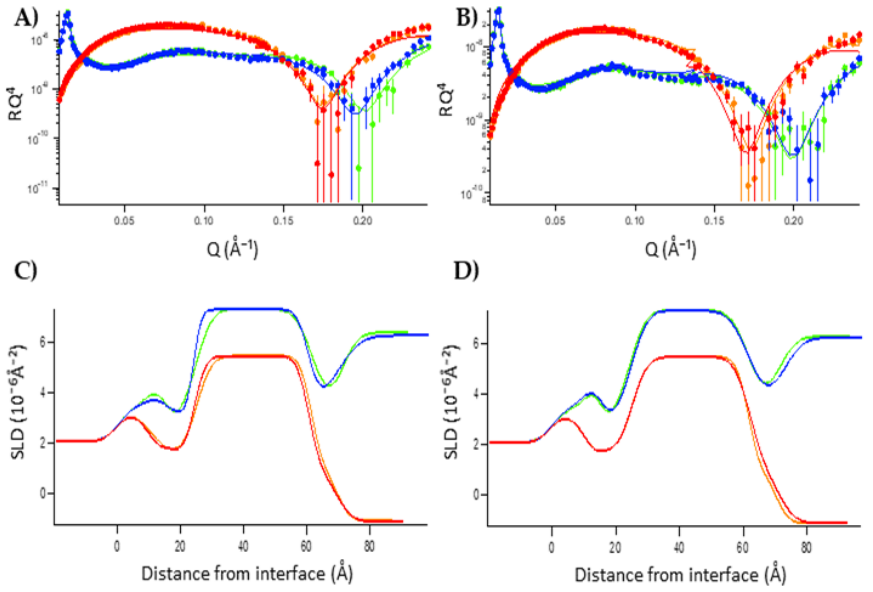

E)

	SLB				SLB + 13-HPOT				SLB + 13-HPOD			
	Thickness (±1 Å)	SLD (±0.05*10⁻⁶ Å⁻²)	Solv P (±5% vol)	Roughness (±2 Å)	Thickness (±1 Å)	SLD (±0.05*10⁻⁶ Å⁻²)	Solv P (±5% vol)	Roughness (±2 Å)	Thickness (±1 Å)	SLD (±0.05*10⁻⁶ Å⁻²)	Solv P (±5% vol)	Roughness (±2 Å)
Solvent	1			5	1			5	1			5
Heads in	10	1,75	32	3	9	1,75	32	4	10	1,75	32	3
Chains in	18	7,66	25	4	17	7,66	25	2	17	7,66	25	4
Chains out	20	766	25	4	19	7,66	25	4	20	7,66	25	4
Heads out	9	1,75	32	4.5	9	1,94	32	3	10	1,87	32	5
		6,36 (D_2O)		4		6,36 (D_2O)		6		6,36 (D_2O)		5
		-0.56 (H_2O)				-0.56 (H_2O)				-0.56 (H_2O)		

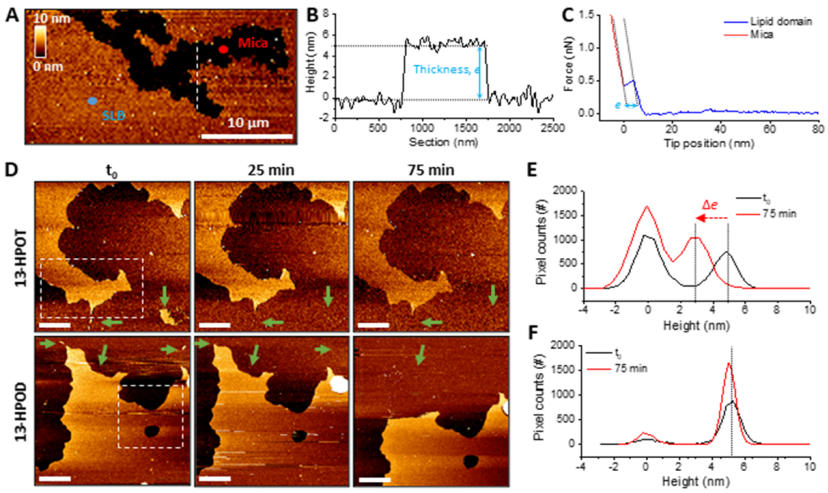

Compound	SLD	Compound	SLD	Compounds	SLD
H_2O	-0.56	PLPC heads PLPC chains	1.93 -0.41	d_{62}-DPPC heads	1,75
D_2O	6.36	Sitosterol	0.22	d_{62}-DPPC chains (gel)	7,66
Si	2.07	GluCer chains	-0.41	d-13-HPOD ($C_{18}D_{32}O_4$)	5.85
SiO_2	3.41	13-HPOD ($C_{18}H_{32}O_4$)	-0.42	13-HPOT ($C_{18}H_{30}O_4$)	-0.56

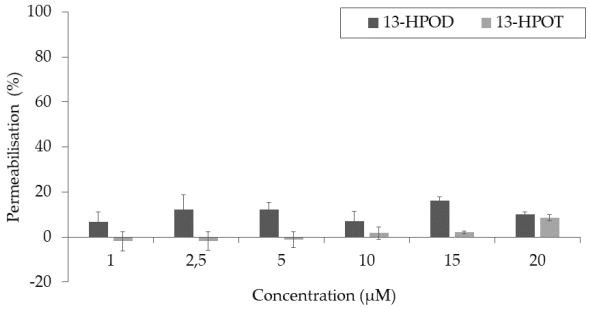

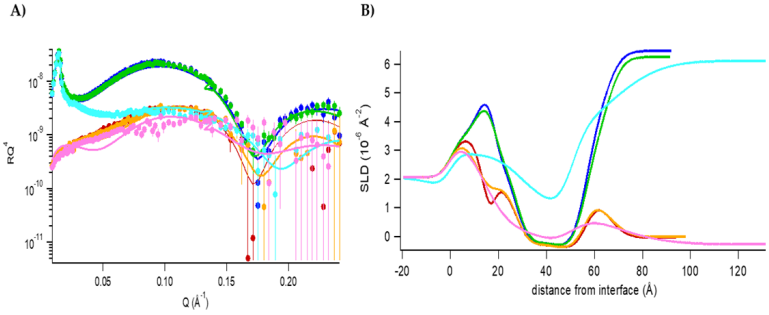

	SLB				SLB + 13-HPOD 1x				SLB + 13-HPOD 3x			
	Thickness (±1 Å)	SLD (±0.05*10⁻⁶Å⁻²)	Solv p (±5% vol)	Roughness (±2 Å)	Thickness (±1 Å)	SLD (±0.05*10⁻⁶Å⁻²)	Solv p (±5% vol)	Roughness (±2 Å)	Thickness (±1 Å)	SLD (±0.05*10⁻⁶Å⁻²)	Solv p ±5% vol)	Roughness (±2 Å)
Solvent	4			5,5	4			6	4			8
Heads in	9	1,98	15	3	10	1,98	15	4	10	1,98	18	14
Chains in	16	-0,28	1	4	16	-0,28	1	4	14	-0,28	5	16
Chains out	13	-0,4	1	4	13	-0,4	1	4	9	-0,4	5	4
Heads out	8	1,93	15	4	9	1,86	15	4	12	1,73	18	5
		6,36 (D_2O)		6		6,36 (D_2O)		7		6,36 (D_2O)		18
		-0.56 (H_2O)				-0.56 (H_2O)				-0.56 (H_2O)		